

Analysis of $p\bar{p}$ in forward and large $|t|$ scattering

A. K. Kohara, E. Ferreira, and T. Kodama

Instituto de Física, Universidade Federal do Rio de Janeiro,

C.P. 68528, Rio de Janeiro 21945-970, RJ, Brazil

The data on $p\bar{p}$ elastic scattering at 1.8 and 1.96 TeV are analysed in terms of real and imaginary amplitudes, in a treatment of very high accuracy, covering the whole t -range and satisfying the expectation of dispersion relation for amplitudes and for slopes. A method is introduced for determination of the total cross section and the other forward scattering parameters and to check compatibility of E-710, CDF and the recent D0 data. Slopes B_R and B_I of the real and imaginary amplitudes, treated as independent quantities, influence the amplitudes in the whole t -range and are important for the determination of the total cross section. New necessary generalized expression is derived for the Coulomb phase. Comparison is made of the values of σ and B_I obtained in forward and full- t approaches, with a new determination of these quantities. The amplitudes are fully constructed, and a prediction is made of a marked dip in $d\sigma/dt$ in the $|t|$ range 3 - 5 GeV² due to the universal contribution of the process of three gluon exchange.

I. INTRODUCTION

The precise knowledge of total cross section and scattering amplitudes in pp and $p\bar{p}$ elastic scattering at high energies is essential for understanding the QCD interactions and hadronic structure, and also for the parametrization and extrapolation of the total cross section that may pass through the LHC measurements and go up to the study of ultra-high energy phenomena in cosmic rays [1]. However, at high energies, due to the smallness of the ratio ρ of the real to the imaginary parts of amplitudes at $t = 0$, together with the absence of data for small $|t|$, turn the extrapolations toward to $|t| \rightarrow 0$ very delicate. It is of fundamental importance to characterize well the $|t| \rightarrow 0$ limits of the scattering amplitudes that are used to determine forward slopes and total cross section.

It is universally understood that the real and imaginary amplitudes in pp and $p\bar{p}$ elastic

scattering amplitudes reflect the non-perturbative QCD dynamics, determined by overall features of the proton and antiproton structures. Regge-like behavior characterizes the s and t dependences at large s and small $|t|$. As a consequence, there appears a dip or an inflection point in the differential cross section $d\sigma/dt$, due mainly to a zero in the imaginary part, and the detailed shape around this region is influenced by the magnitude, sign and form of the real part. An analysis of the interplay of real and imaginary amplitudes is necessary to explain this behavior [2].

In this work, we present a high precision description of the data on $p\bar{p}$ elastic scattering at 1.8 and 1.96 TeV, consistently extended from the forward to the backward regions. This is particularly opportune in view of the publication of the new measurements at 1.96 TeV by the D0 Fermilab experiment [3]. We introduce analytical forms for the amplitudes that are not pure exponentials, and identify their zeros, signs, ranges of dominance and the interplays that fix the details of the observed inflection, dips and bumps. The analytical form of our amplitudes are based on previous studies made in the framework of the Stochastic Vacuum Model [4].

The present work applies previous studies, enriched with the controls offered by dispersion relations for slopes [5] and with the incorporation of new data. Here, we couple the previous 1.8 TeV data with the recent measurements at 1.96 TeV and verify that they are compatible.

It is stressed here that in the analysis of the data, we use information from forward dispersion relations to control parameters of the full description and particularly emphasize the importance of the difference of the slope parameters, B_R and B_I , of the real and imaginary parts. It is commonly assumed in the analysis of data that these slopes are the same, but this is wrong theoretically, and this fact is often overlooked due to the smallness of the ρ parameter. However, when we want to describe consistently the scattering amplitude for the full $|t|$ range, this difference is crucial. Such a description which covers the long t region constrains the quantities of the forward range. This is particularly true and important for the real amplitude that is small with respect to the imaginary part in the forward direction, but not at large $-\text{t}-$. Actually, the differential cross section at high $|t|$ is dominated by the real part.

On the other hand, in the very large $|t|$ domain, the perturbative QCD effects become dominant. We investigate the connection of the measured points at 1.8-1.96 TeV with data of the perturbative tail of large $|t|$ measured at 27 GeV [6]. It is known that this tail is

energy independent and formed by a real amplitude due to three-gluon exchange [7], with opposite signs for pp and $p\bar{p}$ (positive in pp and negative in $p\bar{p}$) scattering. We show that inclusion of such a universal perturbative amplitude leads to a striking prediction for the behavior of the cross section. In $p\bar{p}$ scattering, when added to the non-perturbative positive real part, the perturbative term creates a third zero, located in the region about 3 - 4 GeV². As the imaginary part is less important in this domain, a marked dip is formed with this cancellation.

Our treatment of the whole data with overall high precision leads to definite prediction of the forward scattering parameters in the context of one analytical form. We thus have a determination of the total cross section σ and of the quantities ρ , B_I and B_R (see Eq. (15)). This treatment is compared to the analysis of a subset of forward points in terms of purely exponential amplitudes, in which we obtain different values for σ and B_I (see Eq. (16)). We show that the two determinations are statistically equivalent, and call attention that the discrepancy of the two approaches would be reduced if more data at low $-t$ were available. Thus the determination of σ remains model dependent. Obviously, we advocate that the determination based on the full data is more interesting, since it incorporates properties of curvatures and zeros of the amplitudes.

We organize the present work as follows. In Sec. 2, we present scattering amplitudes that describe the whole $|t|$ range, and the necessary quantities are defined, with a discussion of the role of the universal perturbative amplitude for large $|t|$. In Sec. 3, the precise analysis of the data at 1.8-1.96 TeV to determine all quantities is presented. In Sec. 4, we summarize our results and discuss the prediction introduced in this work. In the Appendix, we derive new expression for the Coulomb phase adapted to incorporate the difference in slope parameters of real and imaginary amplitudes.

II. GENERAL DESCRIPTION OF FORWARD AND FULL t SCATTERING

In the treatment of elastic pp and $p\bar{p}$ scattering in the forward direction, with amplitudes approximated by pure exponential forms, the differential cross section is written

$$\begin{aligned} \frac{d\sigma}{dt} = \pi (\hbar c)^2 \left\{ \left[\frac{\rho\sigma}{4\pi (\hbar c)^2} e^{B_R t/2} + F^C(t) \cos(\alpha\Phi) \right]^2 \right. \\ \left. + \left[\frac{\sigma}{4\pi (\hbar c)^2} e^{B_I t/2} + F^C(t) \sin(\alpha\Phi) \right]^2 \right\}, \end{aligned} \quad (1)$$

where $t \equiv -|t|$ and we have assumed different values for the slopes B_I and B_R of the imaginary and real amplitudes. In the following discussion, we use the unit system where σ is in mb(milibarns) and energy in GeV, so that $(\hbar c)^2 = 0.389 \text{ mbGeV}^2$.

The Coulomb amplitude $F^C(s, t)$ enters for pp/p \bar{p} with the form

$$F^C(s, t)e^{i\alpha \Phi(s, t)} = (-/+) \frac{2\alpha}{|t|} e^{i\alpha \Phi(s, t)} F_{\text{proton}}^2(t) , \quad (2)$$

where α is the fine-structure constant, $\Phi(s, t)$ is the Coulomb phase and the proton form factor is written

$$F_{\text{proton}}(t) = [0.71/(0.71 + |t|)]^2 . \quad (3)$$

In usual treatments of the data, no distinction is made between B_R and B_I slopes, in contradiction with expectations from dispersion relation [5], and a necessary generalization of the commonly used assumption is required. However, when $B_R \neq B_I$, treatment of the Coulomb interference requires a more general expression for the Coulomb phase, which is derived in the appendix.

In elastic pp and p \bar{p} scattering at all energies above $\sqrt{s} = 19 \text{ GeV}$, the real and imaginary amplitudes have zeros located in ranges $|t| \approx (0.1 - 0.3) \text{ GeV}^2$ and $|t| = (0.5 - 1.5) \text{ GeV}^2$ respectively, and the use of exponential forms beyond a limited forward range leads to inaccurate determination of the characteristic forward scattering parameters σ , ρ , B_I and B_R . To obtain precise description of the elastic $d\sigma/dt$ data for all $|t|$, we introduce amplitudes with forms [2]

$$T_R(s, t) = \alpha_R(s) \exp(-\beta_R(s)|t|) + \lambda_R(s) \Psi_R(\gamma_R(s), t) + \sqrt{\pi} F^C(t) \cos(\alpha\Phi) , \quad (4)$$

and

$$T_I(s, t) = \alpha_I(s) \exp(-\beta_I(s)|t|) + \lambda_I(s) \Psi_I(\gamma_I(s), t) + \sqrt{\pi} F^C(t) \sin(\alpha\Phi) , \quad (5)$$

with the shape functions

$$\Psi_K(\gamma_K(s), t) = 2 e^{\gamma_K} \left[\frac{e^{-\gamma_K \sqrt{1+a_0|t|}}}{\sqrt{1+a_0|t|}} - e^{\gamma_K} \frac{e^{-\gamma_K \sqrt{4+a_0|t|}}}{\sqrt{4+a_0|t|}} \right] , \quad (6)$$

where $K = R$ for the real amplitude and $K = I$ for the imaginary amplitude. We here have quantities α_I , β_I , γ_I , λ_I , α_R , β_R , γ_R , λ_R whose roles are explained below. γ_K is dimensionless, while α_K , γ_K and β_K are in GeV^{-2} . These forms have been developed in the application of the Stochastic Vacuum Model to pp and p \bar{p} elastic scattering [2], and the

fixed quantity $a_0 = 1.39 \text{ GeV}^{-2}$ is related to the square of the correlation length of the gluon vacuum expectation value ($a = (0.2 - 0.3) \text{ fm}$) [4].

From the above expression, we can express the total cross section $\sigma(s)$, the ratio ρ of the real to imaginary amplitudes, the slopes $B_{R,I}$ of the amplitudes at $t = 0$, and the differential cross section $d\sigma/dt$ as

$$\sigma(s) = 4\sqrt{\pi} (\hbar c)^2 (\alpha_I(s) + \lambda_I(s)) , \quad (7)$$

$$\rho(s) = \frac{T_R(s, t=0)}{T_I(s, t=0)} = \frac{\alpha_R(s) + \lambda_R(s)}{\alpha_I(s) + \lambda_I(s)} , \quad (8)$$

$$\begin{aligned} B_K(s) &= \frac{1}{T_K(s, t)} \frac{dT_K(s, t)}{dt} \Big|_{t=0} \\ &= \frac{1}{\alpha_K(s) + \lambda_K(s)} \left[\alpha_K(s) \beta_K(s) + \frac{1}{8} \lambda_K(s) a_0 (6\gamma_K(s) + 7) \right] , \end{aligned} \quad (9)$$

$$\frac{d\sigma}{dt} = (\hbar c)^2 |T_R(s, t) + iT_I(s, t)|^2 . \quad (10)$$

We have thus defined the form of the amplitudes for all t at each energy. The parameters must be obtained from phenomenological analysis of the data, with control from dispersion relations for amplitudes and for slopes. The forms of Eqs. (4), (5), (6) are able to describe the imaginary and real amplitudes at all energies, with consistency in their features (magnitudes, signs, locations of zeros), and with smoothness in the energy dependence of the parameters. Values of ρ and B_R must be related with σ and B_I respecting dispersion relations. The forms have been used successfully to represent the data at all energies [2].

This description represents the nonperturbative QCD dynamics that is responsible for soft elastic hadronic scattering. They effectively account for the terms of Regge and eikonal phenomenology that determine the process up to $|t|$ ranges up to about $|t| \approx 2.0 \text{ GeV}^2$. These forms disentangle the imaginary and real amplitudes and are able to reproduce with good accuracy all $d\sigma/dt$ behavior.

In the applications of these forms to phenomenology it was found that the imaginary amplitude presents one zero located in the range $(0.5 - 1.5 \text{ GeV}^2)$. The real amplitude presents one zero at low $|t|$ ($|t| < 0.3 \text{ GeV}^2$), according to a theorem by Martin [8], and a second zero whose location determines the shape of $d\sigma/dt$ around the dip (or inflection point). As a general behavior, we have that the imaginary part Eq. (5) is negative and the real part Eq. (4) is positive for $|t|$ larger than 1.5 GeV^2 . These features are simple and all

data are described accurately. The amplitudes are drawn in the LHS of Fig 1, with marks at their zeros.

It is observed that after the dip (or inflection point) the behavior of the differential cross sections becomes increasingly energy independent. The elastic pp experiment at $\sqrt{s} = 27$ GeV [6] has measured the range from 5.5 to 14.2 GeV² and is the only experiment covering such high values of $-t$. This distribution at high $|t|$ shows remarkable universality: at all energies $\sqrt{s} = 23.5, 30.7, 44.7, 52.8$ and 62.5 GeV, namely at all energies where measurements have reached the intermediate $-t$ region, $d\sigma/dt$ approaches the same set of points of the 27.4 GeV experiment.

The observed $d\sigma/dt$ at the tail has a dependence of form $1/|t|^8$, and has been explained by Donnachie and Landshoff [7] as being of perturbative origin, due to a contribution of three gluon exchange. This term is real and has an amplitude of the form

$$A(s, t)_{ggg} = -\frac{N}{|t|} \frac{5}{54} \left[4\pi\alpha_s(|\bar{t}|) \frac{1}{m^2(|\bar{t}|) + |\bar{t}|} \right]^3, \quad (11)$$

where

$$\alpha_s(|\bar{t}|) = \frac{4\pi}{(11 - \frac{2}{3}N_f) \left[\log \left(\frac{m^2(|\bar{t}|) + \bar{t}}{\Lambda^2} \right) \right]} \quad (12)$$

is the strong coupling constant and $m(|t|)$ is the gluon effective mass [9]. The factor 3 in $\bar{t} \approx (\sqrt{t}/3)^2$ comes from the assumption that each gluon carries one third of the momentum. The normalization factor N is negative and determined by the nucleon structure. To extend our description to include the very high $|t|$ range of this form, we introduce a term $R_{ggg}(t)$, writing

$$T_{R(\text{tail})}(s, t) = \alpha_R(s) \exp(-\beta_R(s)|t|) + \lambda_R(s) \Psi_R(\gamma_R(s), t) + \sqrt{\pi} F^C(t) \cos(\alpha\Phi) + R_{ggg}(t), \quad (13)$$

where $R_{ggg}(t)$ is chosen so that the differential cross section to be dominated by a term of the form $|t|^{-8}$ for large $|t|$ values (say above 2.5 GeV²), while for small $|t|$ the amplitude stays unaltered as the original nonperturbative expression. The perturbative three gluon exchange has opposite signs for pp and $p\bar{p}$ scattering, being positive for pp and negative for $p\bar{p}$. We then take the following expression,

$$R_{ggg}(t) \equiv \pm 0.45 t^{-4} (1 - e^{-0.005|t|^4}) (1 - e^{-0.1|t|^2}), \quad (14)$$

where the signs \pm apply to the pp and $p\bar{p}$ amplitudes respectively. The factor 0.45 is chosen to reproduce the Faissler measurements and the last two factors are written to suppress

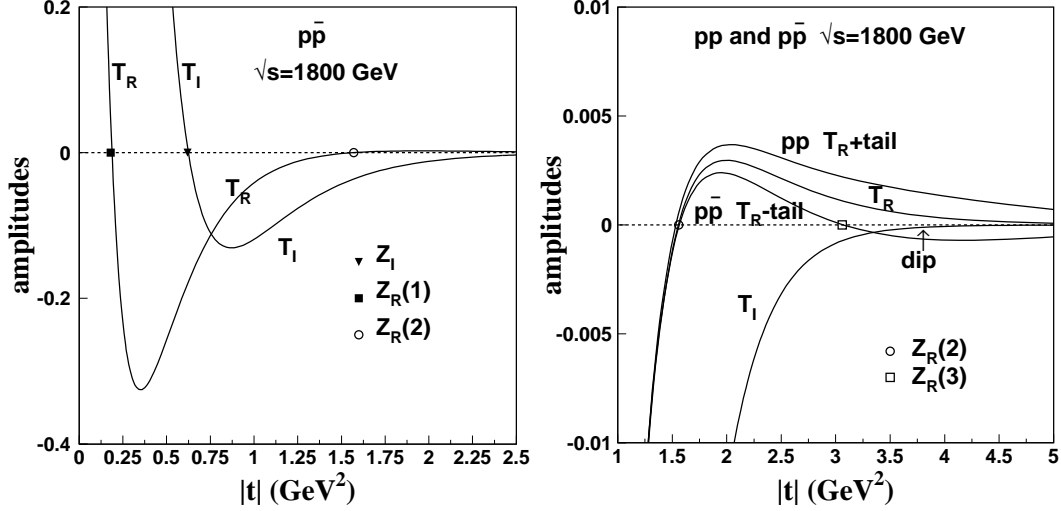


FIG. 1: Amplitudes in pp and $p\bar{p}$ elastic scattering shown in different ranges and scales, described by Eqs. (4), (5), (6) and determined by phenomenology. In the $|t|$ range up to about 2 GeV² the amplitudes are governed by nonperturbative dynamics and are qualitatively similar for the pp and $p\bar{p}$, with one zero for T_I and two zeros for T_R . T_I remains negative and goes fast to zero, while at $|t| \approx 3$ GeV² the nonperturbative T_R is positive and dominates. In $p\bar{p}$ scattering the negative contribution of the 3 gluon exchange term cancels T_R , forming a third zero and a marked dip in $d\sigma/dt$.

smoothly the perturbative contribution for small $|t|$. The transition region from 2 to 5 GeV² contains information on the nature and interplay of nonperturbative and perturbative contributions, which must be investigated.

In the analysis of the scattering amplitudes in the nonperturbative domain, we find that the real amplitude is positive in the transition region, for both pp and $p\bar{p}$ systems. In $p\bar{p}$ scattering, the inclusion of the negative tail amplitude, cancels the positive nonperturbative part, creating a third zero. Then, as the imaginary part is not dominant, a marked dip may be observed in $d\sigma/dt$ in the transition region. This is shown in Fig. 3.

III. ANALYSIS OF ELASTIC $p\bar{p}$ DATA AT 1800 GeV

The available data at 1800 GeV consist of 51 points from the E-710 experiment [10] for $0.0339 \leq |t| \leq 0.627 \text{ GeV}^2$ and 26 points from the CDF experiment [11] for $0.26 \leq |t| \leq 1.26 \text{ GeV}^2$. Recent data at 1.96 TeV [3] from the D0 experiment with 17 points with $0.26 \leq |t| \leq 1.26$ are considered to supersede part of the E-710 data, forming a set of $35+17=52$ points, that we call Set I. The new data from the D0 experiment at 1.96 TeV have here been reduced by a factor $(1.8/1.96)^{0.3232} = 0.973$ based on Regge phenomenology in order to adjust all data to the same 1.8 TeV energy (as the t range involved is small we neglect the $|t|$ dependence of this factor). We merge with these the 26 points from the CDF experiment, that covers about the same range of the 17 D0 points at 1.96 TeV, mounting Set II with 78 points.

The existing data stops at about $|t| = 1.3 \text{ GeV}^2$, leaving the higher $|t|$ region without information and without constraints to fix the connection with the range of the perturbative tail. Thus the parameter β_R cannot be fixed uniquely. As its value is crucial for the prediction of the position and depth of a dip in the transition region for 1.8 TeV, we present two alternative choices, with $\beta_R = 1.15$ and 1.40 . The two solutions have the same values for $\alpha_I, \beta_I, \lambda_I$, (and thus σ), ρ, B_I, B_R . Noting that $\gamma_I, \gamma_R, \alpha_R$ are fixed from other quantities, the fitting of each solution is needed only to provide λ_R . The results are given in Table I, where we observe remarkable quality in the description of the data, with very low $\langle \chi^2 \rangle$ values, smaller than 1.

In a parametrization covering all $|t|$ values using Eqs. (4), (5), (6), we find that sets I and II are compatible with each other, leading to approximately the same numerical values of the parameters. The $\langle \chi^2 \rangle$ values are different in the two cases, because of redundancy of equivalent points (the 26 CDF points and the 17 D0 points are show to be statistically equivalent in their central values) and because of the larger error bars of the CDF data. Thus the more complete Set II has an improved average $\langle \chi^2 \rangle = 0.67$ compared to $\langle \chi^2 \rangle = 0.80$ of Set I.

In what follows we adopt the parameter values obtained with the more complete Set II, with $N = 78$ points. The values of the physical quantities are

$$\sigma = 72.75 \pm 0.18, \quad \rho = 0.138 \pm 0.004, \quad B_I = 16.80 \pm 0.04, \quad B_R = 26.23 \pm 0.37. \quad (15)$$

We recall that the above analysis is based on our analytical expressions applied to all

TABLE I: Quantities of the all- t representation. Common values : $\sigma = 72.75 \pm 0.18$, $\rho = 0.138 \pm 0.0004$, $B_I = 16.80 \pm 0.04$, $B_R = 26.23 \pm 0.37$, $\alpha_I = 12.9632 \pm 0.0248$, $\lambda_I = 13.4156 \pm 0.0399$, $\beta_I = 4.2060 \pm 0.0082$. Set I built with E-710 and D0 data. Set II has additionally the CDF data. The real amplitude parameters β_R and λ_R characterize different solutions. $\langle \chi^2 \rangle$ is the average of squared relative theoretical/experimental deviations.

Set	$\beta_R = 1.15$	$\beta_R = 1.40$
I	$\lambda_R = 3.5714 \pm 0.0094$	$\lambda_R = 3.5628 \pm 0.0105$
N=52	$\chi^2 = 0.80$	$\chi^2 = 0.80$
II	$\lambda_R = 3.5628 \pm 0.0088$	$\lambda_R = 3.5530 \pm 0.0099$
N=78	$\chi^2 = 0.67$	$\chi^2 = 0.67$

$|t|$. We believe that this analysis leads to a reliable determination of the so called forward scattering parameters σ , ρ , B_I , B_R that are characteristic of forward scattering. Our analytical forms intrinsically have curvatures in the amplitudes that allow them to cross zero so that they are able to describe the characteristic structure of $d\sigma/dt$, with dips, bumps and inflection points.

Now, in order to check the sensitivity of our fits of above parameters to the global form of our amplitude, we analyse separately the forward scattering region that usually serves to the determination of σ , ρ , B_I . In such analyses, traditionally the amplitudes at low $|t|$ are described with pure exponential forms as in Eq.(1), and must be restricted to a low $|t|$ range.

The 1.8/1.96 TeV data are poor in the forward direction, and do not include the interval from 10^{-3} to 10^{-2} GeV², with the E-710 data starting at $|t| = 0.0339$ GeV². The CDF data are restricted to the intermediate $|t|$ range, $|t| \geq 0.26$ GeV², and do not give good basis for extrapolation to find the optical point and determine the total cross section.

We select the 24 first points $0.0339 \leq |t| \leq 0.0827$ of the E-710 experiment and fit with 4 parameters using Eq. (1). Using Eq. (1), our results, with $\langle \chi^2 \rangle = 0.62$, are

$$\sigma = 71.92 \pm 0.23 , \rho = 0.138 \pm 0.031 , B_I = 16.20 \pm 0.12 , B_R = 26.23 \pm 9.27 . \quad (16)$$

Thus the parameters of the imaginary amplitude (σ and B_I) are not the same as in the long $|t|$ analysis in Eq.(15) and the larger error bars in ρ and B_R must be noted. The lines representing the two kinds of description of the data are shown in the RHS of Fig. 2.

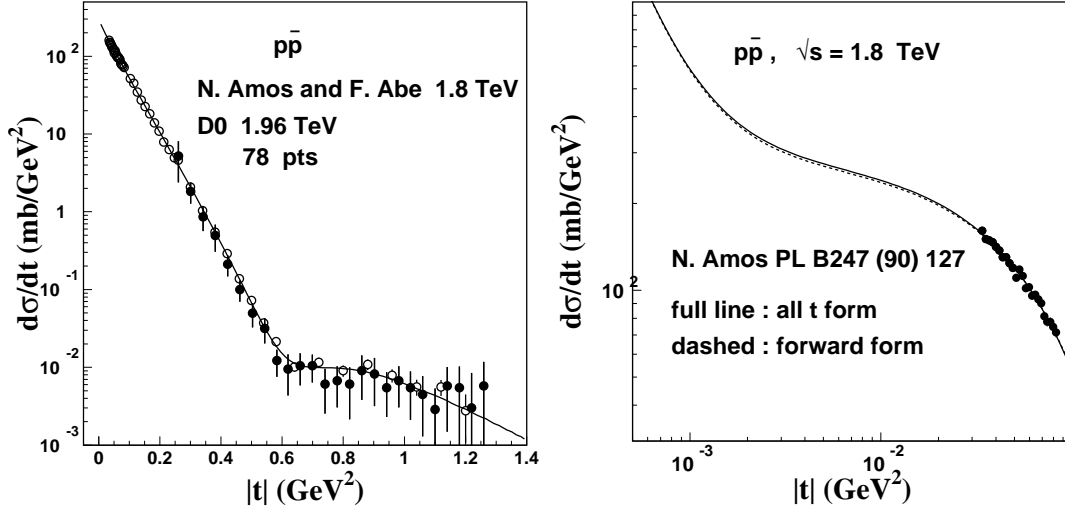


FIG. 2: LHS: Data in $p\bar{p}$ scattering at 1.8 TeV : 35 points from A.Amos et al [10], with 17 points from V.M. Abazov et al [3] (slightly converted from 1.96 to 1.8 TeV) in open circles, and 26 points from F.Abe et al [11] in black circles. In the LHS solid (and another superposed line) show analytical forms that describe the data (see Table I). RHS: the first 24 forward points, with $|t| \leq 0.1 \text{ GeV}^2$ treated with forward scattering form of Eq. (1) in dashed line; solid line represents the same full- t line of the LHS. There is no visible distinction in the range of the experimental points, but the limits $|t| \rightarrow 0$ lead to different values of σ and B_I , given in Eqs. (15) and (16).

We can compare numerically the quality of the two descriptions of the 24 data points. The average squares of relative deviations of theoretical values and data are $\langle \chi^2 \rangle = 0.606$ and $\langle \chi^2 \rangle = 0.613$ for the forward and the long- t forms, respectively. We thus see that the two representations (forward and long- t forms) of these data set are practically equivalent in this domain. Different values of σ (72.75 mb and 71.92 mb) and of B_I (16.80 GeV^{-2} and 16.20 GeV^{-2}) indicate the effect of the use of two different approaches to the idealized $|t| = 0$ limit.

We must notice that the real amplitude parameters ρ and B_R are the same (values suggested by dispersion relations) in Eqs. (15) and (16), because they do not receive strong influence from the points of the set of 24 forward points. Actually these parameters become important in the determination of the properties of the real amplitude only for larger $|t|$.

The ambiguity in the determination of σ and B_I (compare Eqs. (15) and (16)) occurs because the data are poor, inexistent below 0.0339 GeV^2 . It is clear for us that the value of σ reported as output (around 80 mb) from the analysis of the CDF experiment based

TABLE II: The inflection point in $d\sigma/dt$, positions of zeros of the amplitudes, locations of the predicted dip and bump, and ratio characterizing the shape of this dip. All quantities in GeV^2 , except the dimensionless ratio. Integrated elastic cross section $\sigma_{\text{el}} = 16.65 \text{ mb}$

β_R	$ t _{\text{infl}}$	$(d\sigma/dt)_{\text{infl}}$	Z_I	$Z_R(1)$	$Z_R(2)$	$Z_R(3)$	$ t _{\text{dip}}$	$ t _{\text{bump}}$	ratio
GeV^{-2}	GeV^2	mb/GeV^2	GeV^2	GeV^2	GeV^2	GeV^2	GeV^2	GeV^2	
1.15	0.7370	0.010	0.6240	0.1774	1.4447	3.6955	3.7376	4.6869	9.0413
1.40	0.7356	0.010	0.6240	0.1779	1.5744	3.0633	3.3198	4.1457	2.0319

on points $|t| \geq 0.26 \text{ GeV}^2$ must be revised. The energy 1.8/1.96 TeV is important for the parametrization of $\sigma(s)$ and its extrapolation for ultra-high energies. We note that the value derived from the CDF data without desentangling the real and imaginary amplitudes gives an increase in the $\sigma(s)$ curve, whereas our value enters more smoothly in the global behavior of $\sigma(s)$. Obviously we recommend the use of a long $|t|$ description, with proper analytical expression, that can be different from ours, but must have the similar features for the amplitudes such as proper magnitudes, curvatures, zeros and signs.

An additional remark about this question of analytical shapes and roles of limits comes from the observation that if we put the values for $\sigma = 72.75 \text{ mb}$, $B_I = 16.80 \text{ GeV}^{-2}$ (together with ρ and B_R values) in the usual forward amplitudes forms, Eq.(1), we obtain $\chi^2 = 0.744$ for the 24 points, that is formally worse than 0.606 of the direct fitting. We thus read the concept: in a case like this, of poor data at low $|t|$, the parameter values represent $|t| \rightarrow 0$ limits of specific analytical forms, and are to be used associated to the expressions for which they have been found. Thus the values of σ and B_I may be considered as model-dependent. Eq. (1) is not a better model. Actually, with $B_R = B_I$ as usually made, it is wrong.

We recall values of the scattering parameters that are found in papers by experimentalists [12]: $\sigma = 71.71 \pm 2.02 \text{ mb}$, $\sigma_{\text{el}} = 15.79 \pm 0.87 \text{ mb}$, $B = 16.3 \pm 0.3 \text{ GeV}^{-2}$ (and also $B = 16.98 \pm 0.22 \text{ GeV}^{-2}$), $\rho = 0.135 \pm 0.044$). We must remark that B (slope of $d\sigma/dt$) is not the same as B_I , and that $B_R \neq B_I$ gives a different meaning to the parameter ρ .

In Table II we give the values of $|t|$ at the zeros of the amplitudes, and the locations of the dip and bump in $d\sigma/dt$ due to the contribution of the 3-gluon exchange term. The quantity $\text{ratio} = (d\sigma/dt)_{\text{bump}}/(d\sigma/dt)_{\text{dip}}$ that informs about the shape of the dip depends strongly on the values of the parameter β_R , that must be determined by experiment.

IV. SUMMARY AND DISCUSSION

In the present work, we have presented a very precise description of the elastic scattering amplitude for the $p\bar{p}$ collisions, merging the recent 1.96 TeV and the former 1.8 TeV data. We introduce analytical forms for the amplitudes in the full range of $|t|$, and identify their zeros, signs, ranges of dominance and the interplays that fix the observed details. We believe that with our method a more correct determination of the forward scattering parameters at 1.8 TeV can be obtained, together with the global form of the amplitude shown in Fig. 1.

We stress that to determine the total cross section and related observables, we must study the properties of the amplitudes, and not a simple phenomenological presentation of the squared observables as $d\sigma/dt$ which may be misleading : in our practice we found cases of very low χ^2 values for the description of $d\sigma/dt$, obtained from unacceptable amplitudes.

Fig.2 clearly shows how delicate is the extrapolation of experimental data of $d\sigma/dt$ towards $|t| = 0$. Our work revises the values of total cross section and slope parameters that are reported in the literature, suggesting new values.

Our analysis indicates that at 1.8 TeV the imaginary zero is in a region where the real

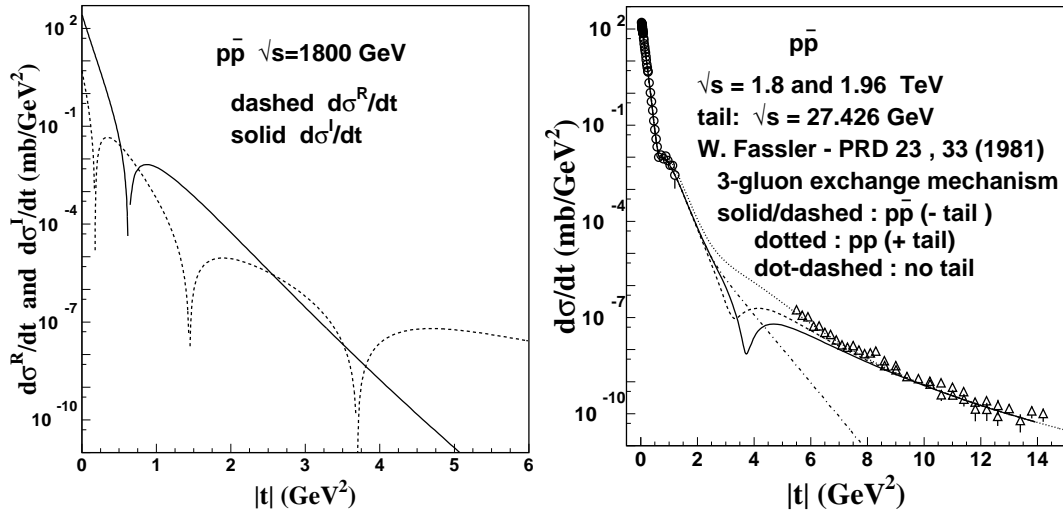


FIG. 3: Predictions for the contributions of real $d\sigma^R/dt$ and imaginary $d\sigma^I/dt$ parts of $d\sigma/dt$ in the presence of the real perturbative tail due to 3 gluon exchange. In $p\bar{p}$ scattering the negative sign of the tail causes a zero in $d\sigma^R/dt$ and a dip in $d\sigma/dt$ located in the range 3-5 GeV^2 . The RHS figure shows two examples of the dip structure, formed with $\beta_R = 1.15$ (solid) and $\beta_R = 1.40$ (dashed) as given in Table I.

part is not weak. Thus there is an inflection point, but not a marked dip as occurs in pp at lower energies. With the increased energy, the imaginary zero has been displaced to lower $-t-$ values more rapidly, and is now distant from the second real zero. The real part is positive and much smaller at $t = 0$, and passes through zero at $|t| \approx 0.2 \text{ GeV}^2$, becoming negative until it crosses zero again, after the inflection point that occurs near 0.74 GeV^2 . The second real zero occurs at $|t| \approx 1.5 \text{ GeV}^2$, while the imaginary part remains always negative after its zero near 0.6 GeV^2 .

For large $-t-$ this real part becomes increasingly dominant over the (negative) imaginary part, that has a rapidly decreasing magnitude. This is the range where the real nonperturbative amplitude dominates. This behavior is observed in Fig. 1, with the line T_R with no tail. We are here in the region of transition between non-perturbative and perturbative dominances. As the nonperturbative real part vanishes, the tail remains, giving to the differential cross section the characteristic shape $1/|t|^8$. This behavior of dip formation is predicted equally for the $p\bar{p}$ cross sections at 541 and 1800 GeV.

The situation is different for $p\bar{p}$ at 52.6 GeV, where the second zero would occur at a higher $|t|$ (about 2 GeV^2) and is not formed due to the action of the negative perturbative tail. At 541 and 1800 GeV the real amplitude become positive before the negative tail enters.

To conclude, we propose an experimental investigation of $d\sigma/dt$ in elastic $p\bar{p}$ scattering in the collected data of the D0 collaboration at values of $|t|$ beyond those already published, where a marked dip may appear. Typical expected results are show in Fig. 3. An observed structure will identify the sign and magnitude of the real amplitude in this region. It becomes clear that the investigation of the transition range from nonperturbative dynamics to the tail region dominated by perturbative contributions is very important.

V. APPENDIX: THE COULOMB PHASE

Here we derive an expression for the phase appropriate for cases with $B_R \neq B_I$.

The starting point is the expression for the phase obtained by West and Yennie [13]

$$\Phi(s, t) = (-/+)\left[\ln\left(-\frac{t}{s}\right) + \int_{-4p^2}^0 \frac{dt'}{|t' - t|} \left[1 - \frac{F^N(s, t')}{F^N(s, t)}\right]\right], \quad (17)$$

where the signs $(-/+)$ are applied to the choices $pp/p\bar{p}$ respectively. The quantity p is the proton momentum in center of mass system, and at high energies $4p^2 \approx s$.

For small $|t|$, assuming that $F^N(s, t')$ keeps the same form for large $|t'|$ (this approximation should not have practical importance for the results), we have

$$\begin{aligned} \frac{F^N(s, t')}{F^N(s, t)} &= \frac{F_R^N(s, 0)e^{B_R t'/2} + i F_I^N(s, 0)e^{B_I t'/2}}{F_R^N(s, 0)e^{B_R t/2} + i F_I^N(s, 0)e^{B_I t/2}} \\ &= \frac{c}{c+i} e^{B_R(t'-t)/2} + \frac{i}{c+i} e^{B_I(t'-t)/2}, \end{aligned} \quad (18)$$

where

$$c \equiv \rho e^{(B_R - B_I)t/2}. \quad (19)$$

The calculation is explained in detail in the appendix. The integrals that appear in the evaluation of Eq. (17) are reduced to the form [14]

$$I(B) = \int_{-4p^2}^0 \frac{dt'}{|t' - t|} \left[1 - e^{B(t'-t)/2} \right], \quad (20)$$

that is solved in terms of exponential integrals [15] as

$$I(B) = E_1\left[\frac{B}{2}(4p^2 + t)\right] - E_i\left[-\frac{Bt}{2}\right] + \ln\left[\frac{B}{2}(4p^2 + t)\right] + \ln\left[-\frac{Bt}{2}\right] + 2\gamma. \quad (21)$$

The real and imaginary parts of the phase are then written

$$\Phi_R(s, t) = (-/+)\left[\ln\left(-\frac{t}{s}\right) + \frac{1}{c^2 + 1}\left[c^2 I(B_R) + I(B_I)\right]\right], \quad (22)$$

and

$$\Phi_I(s, t) = (-/+)\frac{c}{c^2 + 1}\left[I(B_I) - I(B_R)\right]. \quad (23)$$

With σ in mb and t in GeV^2 , the practical expression for $d\sigma/dt$ in terms of the parameters σ , ρ , B_I and B_R is

$$\frac{d\sigma}{dt} = \pi (\hbar c)^2 \left[\left[\frac{\rho \sigma e^{B_R t/2}}{4\pi (\hbar c)^2} + F^C e^{\alpha \Phi_I} \cos(\alpha \Phi_R) \right]^2 + \left[\frac{\sigma e^{B_I t/2}}{4\pi (\hbar c)^2} + F^C e^{\alpha \Phi_I} \sin(\alpha \Phi_R) \right]^2 \right]. \quad (24)$$

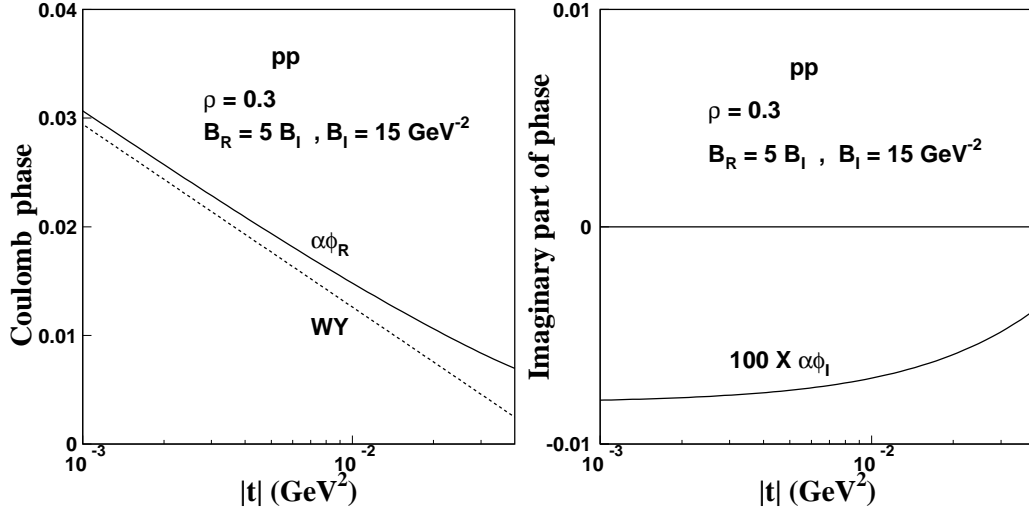
At high energies and small $|t|$ we simplify

$$4p^2 + t \rightarrow s$$

and then the functional form of $I(B)$ is written

$$I(B) = E_1\left(\frac{Bs}{2}\right) - E_i\left(-\frac{Bt}{2}\right) + \ln\left(\frac{Bs}{2}\right) + \ln\left(-\frac{Bt}{2}\right) + 2\gamma. \quad (25)$$

FIG. 4: Comparison of the Coulomb phase $\alpha\Phi_R$ from our calculation of Eq. (22) with the West-Yennie WY expression in Eq. (17). The unrealistic large values of parameters $\rho = 0.3$ and $B_R/B_I = 5$ are chosen in order to enhance differences. The calculation is made at $\sqrt{s}=50$ GeV, but the values of $\alpha\Phi_R(s, t)$ do not show explicit dependence on s up to the LHC energy. The plot of $\alpha\Phi_I$ in the RHS shows extremely small values (notice the scale), about 100 times smaller than $\alpha\Phi_R$, so that we can safely put $\alpha\Phi_I$ equal to zero in Eq.(24).



The expression for the phase $\alpha\Phi_R$ can be compared with the usual expression from West and Yennie

$$\alpha\Phi_{WY} = (-/+)\alpha \left[\gamma + \ln \left(-\frac{Bt}{2} \right) \right]. \quad (26)$$

A numerical comparison is presented in Fig. 4, where we choose *strong* unrealistic parameter values $\rho = 0.3$, $B_R/B_I = 5$ to enhance possible differences, and the lines are drawn for $B_I = 15 \text{ GeV}^{-2}$, with the $d\sigma/dt$ slope B of the WY formula taken as given by

$$B = \frac{\rho^2 B_R + B_I}{1 + \rho^2}. \quad (27)$$

At the high energies of our interest, the phase is insensitive to s .

The plot of $\alpha\Phi_I(s, t)$ in the RHS of Fig. 4 shows that its values are extremely small so the the imaginary part of the phase can be safely put equal to zero.

VI. ACKNOWLEDGMENTS

The authors wish to thank CNPq, PRONEX and Faperj for financial support. A part of this work has been done while TK stayed as a visiting professor at EMMI and FIAS

at Frankfurt. TK expresses his thanks to the hospitality of Profs. H. Stoecker and D. Rischke. Conversations with M. Rangel and G. Alves, of the D0 Collaboration are gratefully acknowledged.

-
- [1] G. Antchev et al.(TOTEM Collaboration), *Europhys. Lett.* **95**, 41001 (2011); id *Europhys. Lett.* **96**, 21002 (2011); M.G. Ryskin, A. D. Martin and V. A. Khoze, *Eur. Phys. J. C* **72**, 1937 (2012) ; I. M. Dremin and V. A. Nechitailo, *Phys. Rev. D* **85**, 074009 (2012); The Pierre Auger Collaboration, Physical Review Letters, in press, 2012.
 - [2] E. Ferreira and F. Pereira, *Phys. Rev. D* **59** , 014008 (1998) ; *Phys. Rev. D* **61**, 077507 (2000).
 - [3] V. M. Abazov et al, D0 Coll., *Phys. Rev. D* **86** , 012009 (2012).
 - [4] H.G. Dosch, E. Ferreira, A. Kramer *Phys. Rev. D* **50**, 1992 (1994) .
 - [5] E. Ferreira, *Int. J. Mod. Phys. E* **16**, 2893 (2007).
 - [6] W. Faissler et al. , *Phys. Rev. D* **23**, 33 (1981).
 - [7] A. Donnachie, P. Landshoff *Zeit. Phys. C* **2**, 55 (1979), *Phys. Lett. B* **387**, 637 (1996).
 - [8] A. Martin, *Phys. Lett.B* **404**, 137 (1997).
 - [9] J. M. Cornwall, *Phys. Rev. D* **26**, 1453 (1982).
 - [10] N. Amos et al, Fermilab E-710 Coll, *Phys. Lett. B* **262**, 127, (1990).
 - [11] F. Abe et al. , Fermilab CDF Coll., *Phys. Rev. D* **50**, 5518 (1993).
 - [12] C. Avila et al., *Phys. Lett.B* **445**, 419 (1999); *Phys. Lett.B* **537**, 41 (2002) .
 - [13] G. B. West and D. Yennie , *Ann. of Phys.* **3**, 190 (1958).
 - [14] V. Kundrať and M. Lokajicek, *Phys. Lett. B* **611**, 102 (2005); V.Kundrať, M.Lokajicek and I. Vrococ, *Phys. Lett. B* **656**, 182 (2007).
 - [15] M. Abramowitz and I. Stegun, *Handbook of Mathematical Functions*.